Physica Medica 68 (2019) 132–145

Contents lists available at ScienceDirect

Physica Medica

journal homepage: www.elsevier.com/locate/ejmp

Review paper

A guide to ^{90}Y radioembolization and its dosimetry

S. Peter Kim[a,*], Claire Cohalan[b], Neil Kopek[c], Shirin A. Enger[a,d,e]

[a] Medical Physics Unit, McGill University, Montreal, Quebec H4A 3J1, Canada
[b] Department of Physics and Biomedical Engineering, CHUM, Montreal, Quebec H2C0X1, Canada
[c] Department of Radiation Oncology, McGill University Health Centre, Montreal, Quebec H4A 3J1, Canada
[d] Department of Oncology, McGill University, Montreal, Quebec, H4A 3J1, Canada
[e] Research Institute of the McGill University Health Centre, Montreal, Quebec H3H 2L9, Canada

ARTICLE INFO

Keywords:
Radioembolization
Dosimetry
^{90}Y
Clinical Background

ABSTRACT

Radioembolization gains continuous traction as a primarily palliative radiation treatment for hepatic tumours. A form of nuclear medicine therapy, Yttrium-90 containing microspheres are catheter guided and injected into the right, left, or a specifically selected hepatic artery. A multitude of comprehensive planning steps exist to ensure a thorough and successful treatment. Clear clinical and physiological guidelines have been established and nuclear imaging is used to plan and verify dose distributions. Radioembolization's treatment rationale is based on tumour and blood vessel dynamics that allow a targeted treatment approach. However, radioembolization's dosimetry is grossly oversimplified. In fact, the currently utilized clinical dosimetric standards (e.g. partition method) have persisted since the 1990s. Moreover, the multitude of radioembolization's intertwining components lies disjointed within the literature. Particularly relevant to new readers, this review provides a methodical guide that presents the treatment rationale behind every clinical step. The emerging dosimetry methods and its factors are further discussed to provide a comprehensive review on an essential research direction.

1. Introduction

Radioembolization, selective internal radiation therapy (SIRT), intra-arterial radiation therapy, or trans-arterial radioembolization (TARE) are all various names for the same clinical procedure. Radioembolization is a specific type of nuclear medicine therapy used to treat primary or metastasized hepatic tumours. It is administered when other minimally invasive treatments have failed and is primarily palliative. During treatment, a catheter is used to guide and inject Yttrium-90 (^{90}Y) containing microspheres into the right, left, or a specifically selected hepatic artery. Due to unique hepatic blood flow, the microspheres are distributed preferentially to the tumour arteries, where they are permanently deposited. The tumour is then irradiated by the particles emitted by ^{90}Y.

^{90}Y is a pure beta-emitter with a half-life of 64.04 hours that disintegrates into stable zirconium-90 (^{90}Zr) by emitting beta particles with a maximum energy of 2.27 MeV and an average energy of 0.937 MeV. Within soft tissue, the released beta energy has a maximum penetration range of 11 mm with an average range of 2.5 mm. Since ^{90}Y deposits most of its energy within the first few millimeters, its therapeutic dose is concentrated at the microspheres location [1]. Currently, there are two commercially available ^{90}Y microsphere products, the glass (Therasphere; BTG plc, UK) and resin microspheres (SIR-spheres; Sirtex Medical Limited, North Sydney, Australia). Both of these spheres are biocompatible, but not biodegradable. Theraspheres have average diameters of 20–30 μm with a standard activity that may range from 3 GBq to 20 GBq per vial. Within a vial of 3 GBq, there are around 22,000 to 72,000 microspheres per milligram, resulting to an average activity of 2500 Bq per microsphere [2,3]. In contrast, the diameters of SIR-spheres range from 20 to 60 μm with an average activity of 50 Bq per microsphere. Normally, each resin vial has a standard activity of 3 GBq and a range of 30–50 million microspheres [2,4]. Highlights between the two differing microsphere products can be seen in the European Association of Nuclear medicine (EANM) guidelines [5]. Contained within pre-packaged vials, both types of ^{90}Y microspheres are delivered, then their activity is measured right before treatment.

Radioembolization involves multiple clinical steps spanning over numerous multidisciplinary fields. There exists a plethora of articles on this treatment modality, yet there is a lack of a study that comprehensively describes the rationale behind the entire radioembolization process. Overall, this review has two objectives. The first aim is to provide a full scope of radioembolization that ties together the rationale and background behind every treatment step. Building on the discussed background, the second aim is to provide a comprehensive review by

* Corresponding author.
E-mail address: shingyu.kim@mail.mcgill.ca (S.P. Kim).

https://doi.org/10.1016/j.ejmp.2019.09.236
Received 5 February 2019; Received in revised form 15 September 2019; Accepted 17 September 2019
Available online 28 November 2019

presenting the most relevant literature related to patient specific radioembolization treatments and its newly emerging dosimetry.

2. Methods

As a multi-disciplinary and multi-step treatment, the topics of emphasis were purposefully constrained to patient-based studies and image-based dosimetry; therefore, only 97 of around 130 original sources were listed to provide a comprehensive and succinct discussion on radioembolization. To provide the understanding and rationale behind each treatment process, background articles on liver vasculature, related nuclear imaging modalities, current clinical dosimetry methods, novel clinical studies, and review articles were included. Search words such as “patient based radioembolization”, “imaged based radioembolization”, “post-image dosimetry” “radioembolization”, “PET/CT”, “SPECT/CT”, “angiography”, and “primary radioembolization treatments” were inputted into specific databases. The most common databases used were Pubmed and WorldCat.

3. Results and discussion

A relatively complete picture of radioembolization can be obtained by reading from the list of suggested articles within Appendix A Table 1. It is important to note that each of the suggested articles assumes a certain level of familiarity and only provides insight into selective segments of this treatment. In other words, none of the presented studies provide a comprehensive overview of every treatment step. Furthermore, dose response effect studies based on clinical dosimetric methods are not included in this review due to the rationale that emerging image based dosimetry methods are more dosimetrically representative. However, a previous review has amassed such results [6].

3.1. Treatment overview

Radioembolization requires planning that involves patient evaluation and pre-treatment imaging, the treatment itself, and finally, shortly after the treatment is completed, post-treatment verification. The multiple clinical steps are listed in Fig. 1. To start, patients are clinically examined for relative and absolute contraindications such as insufficient liver function or extensive and untreated portal hypertension [5]. After a clinical evaluation, patients undergo further preliminary steps that include imaging with a triple phase computed tomography (CT) and/or magnetic resonance imaging (MRI) to assess the liver for liver patency, extrahepatic disease, and tumoural and non-tumoural volumes [6]. Since radioembolization is artery based, pre-treatment workups include an angiography as well as planar scintigraphy imaging (planar imaging) and single photon emission computed tomography (SPECT) co-registered with CT (SPECT/CT) for injected ^{99m}Technetium-magroaggregated albumin (Tc-MAA). Tc-MAA images are used to verify vessel mapping and to visualize any additional arteries that may lead to extrahepatic microsphere distribution. Tc-MAA distribution is also used to calculate what is called the lung shunting percentage or lung shunting fraction (LSF). The LSF estimates the total ^{90}Y microsphere deposition within the lungs and quantifies the risk of developing radiation pneumonitis, a serious side effect. Consequently, radioembolization has lung safety thresholds; if the LSF is too high, patients are deemed ineligible for treatment.

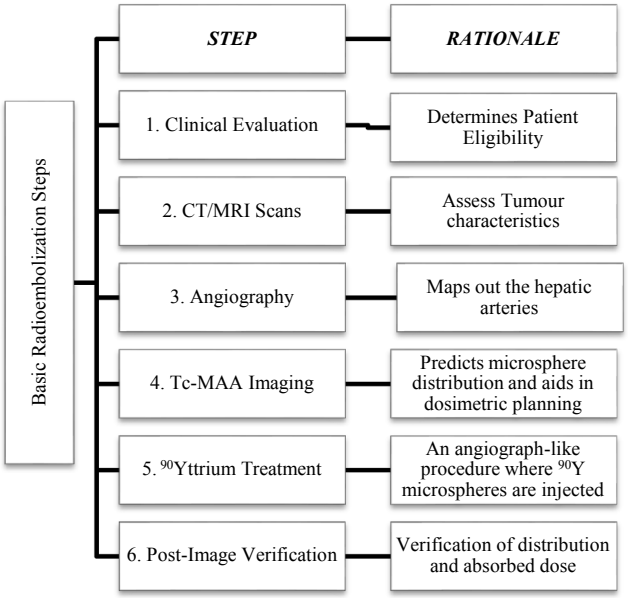

Fig. 1. Clinical steps involved in the ^{90}Y radioembolization process.

During the treatment itself, an interventional radiologist places a catheter percutaneously via a patient’s femoral artery and guides it to the correct hepatic artery under x-ray fluoroscopy. Connected to the catheter, a vial containing ^{90}Y microspheres is infused into the body. Differences exist in the administration of the two different microsphere products. Due to their higher embolic tendency (See 3.8 Treatment), ^{90}Y resin microspheres are successively infused with saline and 5% dextrose whereas glass microspheres are infused by saline alone [7–10]. Recently, an alternate transradial approach has been deemed feasible. This approach involves a catheter placement via a patient’s radial artery and demonstrates advantages such as patient preferability and lower cost, albeit with greater technical challenges [11]. Directly after treatment, the patient has follow-up imaging with SPECT/CT or PET/CT scans to check for the microsphere distribution and to verify the dose. The review of the different treatment steps will be discussed in detail in the coming subsections.

3.2. Patient eligibility

Prior to radioembolization, patients must be deemed suitable for treatment. Radioembolization is used as a primarily palliative treatment, i.e. to preserve the functional capacity of the hepatic tissue [12]. Eligibility stems from the existing functionality and the potential radiation tolerance of a patient’s hepatic parenchyma. Such predictions are divided into three sections indicating when a patient should have treatment, when patient treatment is possible, or when a patient is ineligible for treatment. These indications are respectively labeled indications, relative contraindications, and absolute contraindications. Patient eligibility can be particular to different steps of the treatment plan. In many cases a patient may be eligible under the initial clinical evaluation, but later become ineligible during the pre-treatment imaging workup step of radioembolization [7].

In general, most articles refer to the Radioembolization Brachytherapy Oncology Consortium (REBOC) guidelines and manufacturing recommendations when discussing radioembolization patient selections [3,4,13]. The EANM has also complied patient selection guidelines for the treatment of liver cancer and metastases [5]. The important patient indications include an unequivocal and measurable liver tumour based on CT/MRI scans, a liver-dominant tumour burden, and a life expectancy of at least 3 months [7,13].

Radiation dose to organs at risk is assessed through pre-treatment imaging with an angiography and Tc-MAA to avoid severe side effects such as radiation pneumonitis, gastrointestinal ulceration, and/or gastrointestinal bleeding due to extrahepatic microsphere deposition [14]. Patients are further ineligible for treatment if they have factors such as a compromised portal vein, are pregnant, or have liver failure [7,13]. The treatment eligibility has relative contraindications as well, which are based on a case-by-case basis and left to the discretion of the physician. Some factors include patients with a limited hepatic reserve, poor kidney function, or an Eastern Cooperation Oncology Group

Table 1
ECOG performance ranking description.

Grade	ECOG Performance Status
0	Fully active, able to carry on all pre-disease performance without restriction
1	Restricted in physically strenuous activity but ambulatory and able to carry out work of a light or sedentary nature, e.g., light house work, office work
2	Ambulatory and capable of all self-care but unable to carry out any work activities; up and about more than 50% of waking hours
3	Capable of only limited self-care; confined to bed or chair more than 50% of waking hours
4	Completely disabled; cannot carry on any self-care; totally confined to bed or chair
5	Dead

(ECOG) performance status of 2–4 [7,13,15]. Grading levels of the ECOG status are explained in Table 1. However, age and prior surgical resection are not considered to be contraindications, making radioembolization appealing for palliative therapy [16].

With restricting clinical factors well set for radioembolization, there are ideal patients who are predicted to have a good tolerance to the treatment. These patients normally show an ECOG status of less than 2, normal bilirubin levels, normal liver synthetic function (albumin greater than 3 mg/dL), a lack of ascites, and less than 50% tumour burden [7]. It has been shown that ECOG status rather than a tumour's clinical stage is the more reliable factor in a patient's treatment tolerance [15]. For metastatic tumours, lower bilirubin levels were also found to be reliable indicators for radioembolization tolerance [15,16]. Overall criteria and specificities of eligibility are presented in Table 2. For ^{90}Y treatment, it should be stated that the institutional and corresponding product eligibilities should always be consulted [3,4].

3.3. Standard liver vasculature

As the name implies, radioembolization is built around the hepatic vasculature where the injected radioactive microspheres travel and permanently localize within the hepatic arteries. Macroscopically, hepatic vascularization is comprised of a dual blood supply where the portal vein provides 75–80% of the hepatic blood supply and the hepatic arteries provide 20–25% of the blood [17,18]. The portal vein provides partly deoxygenated but nutrient rich blood to the liver from the gastrointestinal tract while the hepatic arteries provide the oxygenated blood [17]. Branches of the portal vein further divide and pass between hepatic lobules and eventually end up as sinusoids. Lobules are hexagonally functional units of the liver, otherwise known as hepatic parenchyma, and contain hepatocytes, bile of canaliculi, sinusoids, and a central vein. Hepatic tumours almost exclusively derive their blood supply from the hepatic arteries while the normal parenchyma is perfused through the portal veins. For a more thorough physiological investigation on hepatic perfusions, reviewing Van de Wiele (2012) is suggested [19]. With preferential hepatic perfusion being the basis for radioembolization, select hepatic artery catherization provides a way for the microspheres to target malignant hepatic tumours while sparing the normal tissue [18]. Therefore, a background on the most common hepatic vasculature is given.

The standard hepatic vasculature scheme starts with the celiac axis [20]. The first major branch off the aorta, the celiac artery then trifurcates into the left gastric artery (LGA), splenic artery, and the common hepatic artery (CHA). From there, the CHA continues to bifurcate into the proper hepatic artery (PHA) and the gastroduodenal artery (GDA) and more distally the PHA divides into the right and left hepatic arteries at the hilar plate. Moreover, both hepatic arteries continually branch and decrease in size to perfuse the hepatic parenchyma and eventually make up the microvasculature of the hepatocytes, which is later discussed in 3.11 Liver Microcirculation & Distribution. Fig. 2 illustrates an example of a patient's hepatic vasculature.

Table 2
Patient Eligibility Specifications.

Ideal Patient
1. ECOG < 2
2. No ascites
3. Less than 50% tumour burden
4. Albumin > 3 mg/dl
5. Bilirubin < 2 mg/dl

Indications
1. CT/MRI established Tumour
2. Liver Dominant Tumour
3. Life Expectancy > 12 weeks

Relative Contraindications
1. Excessive tumour burden without hepatic reserve
2. Compromised Portal Vein when super-selective catherization cannot be performed
3. Prior radiotherapy
4. ECOG 2–4
5. Creatine > 2.5 mg/dl
6. Abnormal bone marrow function
7. Bilirubin levels (> 2 mg/dl) with no reversible cause

*Absolute Contraindications**

Clinical Evaluation
1. Ascites and/or other symptoms of liver failure
2. Pregnant
3. Capecitabine last 2 months or planned to be administered in the future

Tc-MAA Imaging
1. > 30 Gy predicted to lungs or > 20% LSF**
2. Any extrahepatic deposition within the gastrointestinal tract
3. Extensively compromised Portal Vein
4. For repeated treatments, a 50 Gy cumulative lung dose should not be surpassed**

* Steps are based on Fig. 1.
** See 3.9 Current Clinical Dosimetric Methods for Gy value explanations.

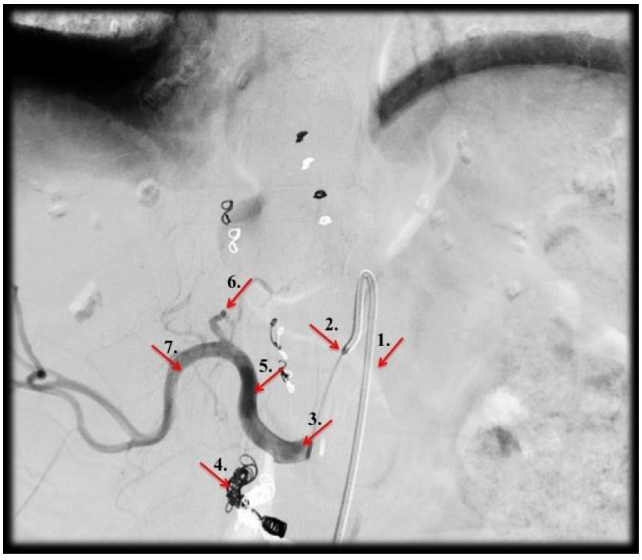

Fig. 2. A digital subtraction angiography is shown for a patient being planned for right lobe radioembolization. The different parts of the hepatic vessels are labeled: 1. Catheter in the celiac trunk, 2. Micro-catheter that is extended to 3. The common hepatic artery, 4. A gastroduodenal artery that is coil embolized, 5. Proper hepatic artery, 6. Left hepatic artery, 7. Right hepatic artery.

3.4. Angiography

In an ideal scenario, radioembolization microspheres will localize solely within the hepatic tumour's vasculature. In reality, radioembolization microspheres localize within both the healthy and tumour liver tissue. Many variations exist within the overall hepatic vasculature that may lead to additional complications. In fact, hepatic vessel variations are quite common and can be expected in 45% of patients [21]. If such vessel variations do exist, the variable hepatic vasculature may cause extrahepatic deposition, which results in the irradiation of non-hepatic healthy tissue.

Due to such variations in vasculature, an angiography is used to map patient-specific arteries [20,22]. The goal of an angiographic evaluation is three fold: it is to guide the delivery catheter positioning, evaluate pre-treatment blood flow, and to determine the variant arteries that may lead to extrahepatic microsphere deposition [8,13]. Van den Hoven et al. (2014) found that only 49% of patients had their aberrant hepatic arteries correctly identified from a standard CT scan and only 86% during angiography [20]. Thus, several modifications were recommended to the standard process including, but not limited to the use of a multiphase liver CT before an angiography, the use of C-arm cone beam CT, catheter-directed CT angiography (CTA), and an evaluation of SPECT/CT co-registered images from Tc-MAA [20,23].

Once an angiography has been performed and possible variant vessels identified, coil embolization (also called coil occlusion or skeletonization) is recommended [8,13,15,23]. Coil embolization involves a catheter and a metal cable that has attached collagen fibres. The metal cable is pre-formed as a spiral that is set straight. When released from a catheter, the pre-straightened coil spirals into its natural form that occludes most of the aberrant vessel. The attached collagen fibres then induce thrombosis, which blocks the rest of the vessel and prevents unwanted microsphere deposition. Coil embolization in turn directs microsphere flow to the targeted region. Depending on the variant arteries, the size of the arteries, and possible angiographic preferences, coil embolization is a calculated choice. On one hand, prophylactic embolization is seen as the safer option as the dangers of grave clinical complications such as gastrointestinal ulceration and bleeding outweigh the dangers of coil embolization [15]. On the other, coil embolization is avoided in the most experienced centers due to complications and limited benefits of an embolized treatment [24]. At our institution, coil embolization is administered when necessary such as when shunts to the gastrointestinal track are visible. Fig. 2 further demonstrates an angiogram and the relevant vessels for a patient being treated for radioembolization.

Coil embolization's effectiveness depends on the patient's coagulation speed and the effectiveness of the actual embolization. In some patients, their de-coagulation speed may be faster than others when the induced thrombosis is cleared up and blood flow is resumed (re-canalization). In others, the initial coils may not have been packed tight enough to induce thrombosis in the first place. This problem is easily remedied through additional packing of coils. Moreover, some patients may have new vessels (collaterals) develop leading to resumed blood flow back to the targeted organ. Whatever the case, the best preparation method must be determined and evaluated for a patient undergoing radioembolization treatment.

3.5. Tc-MAA pre-treatment imaging

After an angiography, Tc-MAA is used to predict the potential distribution of ^{90}Y microspheres. Tc-MAA is normally provided in a vial of 10 ml solution containing 4.8 x10^6 aggregated albumin particles where 90% or more are between 10 and 90 μm in diameter. The particles may measure outside such parameters, but still have a maximum range from 0 to 150 μm [8]. With a short physical half-life of 6 hours and a continual bio-degradation of ^{99m}Tc from MAA, it is recommended that the Tc-MAA imaging to be done at least within 60 minutes of administration. An adult activity consists of 185 MBq Tc-MAA suspended in normal saline. If the whole liver is treated, the right and left hemilivers will be injected with 111 MBq and 74 MBq, respectively [23].

After injection, a gamma detection system produces a whole-body image. Planar imaging may be used to assess Tc-MAA depositions, but studies suggest a tomographic imaging modality such as a SPECT scan or a combination of SPECT and CT to provide a more accurate check of the Tc-MAA bio-distribution [13]. It was found that planar imaging might not provide adequate detection, especially when extrahepatic sites or a non-homogenous Tc-MAA distribution is present. However, planar imaging is still clinically adopted although SPECT/CT has been proven to be more accurate for determining the distribution of Tc-MAA and the quantification of its LSF [25–27].

The Tc-MAA image is then compared to the previously assessed angiograph where the injected particle distribution is compared to the pre-planned vasculature. Ideally, the Tc-MAA microspheres are all contained within the imaged angiographic vasculature; however, the Tc-MAA microsphere distribution and the angiographically predicted distribution can differ [23]. There are multiple causes for this discrepancy. A catheter may have been misplaced distally or past the branching point that excludes the part of the liver to be treated. New parasite vessels may have sprouted between the time the angiography was performed and the time Tc-MAA was injected. A hepatic artery may have been missed during the angiographic treatment. If any of the above scenarios are illustrated, a second angiography and a subsequent Tc-MAA injection is recommended to confirm the new vascularization [28]. Additionally, extrahepatic activity may be seen from Tc-MAA. To combat unwanted extrahepatic activity, solutions such as additional coiling, more distal placement of the catheter, and/or super selective catherization (radiation segmentectomy) during treatment are further suggested. Coiling would physically block the ^{90}Y microspheres from passing through a specific vessel. More distal catheter placement prevents less reflux of microspheres, if any, due to the catheter physically being farther from any arterial branching. Similarly, super-selective catherization keeps microsphere localization within specifically perfused segments within the liver (for further detail see 3.8 Treatment).

On top of overall vessel discrepancies, the distribution within the same vasculature may have unusual Tc-MAA accumulations in both extrahepatic and intrahepatic sites [23]. To plan a safe treatment, awareness of this heterogeneous distribution is needed to attribute a specific distribution to a cause. A variety of factors such as presence of necrotic lesions, prior trans-arterial chemoembolization (TACE) treatments, invasion of tumour within hepatic arteries, aggregation of Tc-MAA particles, or variable flow dynamics within the liver may result in heterogeneous distribution. Proficient knowledge on the causes of discrepant Tc-MAA distributions and the necessary steps to combat them is required for an accurate radioembolization treatment plan and later, if calculated, for its dosimetry.

3.6. The lung shunt fraction (LSF)

Theoretically, the ^{90}Y microspheres should embolize within the tumour's hepatic terminal arteries (See 3.11 Liver Microcirculation & Distribution). However, arteriovenous blood vessel shunts may provide ^{90}Y microspheres a direct vascular path to the lungs, which may then cause lung irradiation [13]. To predict this, Tc-MAA distribution is used to calculate the LSF. Estimated by the ratio of counts in the lungs to the summed counts in the lungs and liver, the LSF uses planar imaging or SPECT/CT count data for its calculations. In other words, the LSF is the fraction of Tc-MAA particles that made its way into the lungs due to arteriovenous shunts. It is worth noting that there are variations in size, density, and number between Tc-MAA particles and ^{90}Y microspheres; however, Tc-MAA particles are still used to predict the undesirable ^{90}Y microsphere deposition within the lungs. [23].

Depending on the imaging modality used, there exist limitations

that can affect the calculation of the LSF [29]. Planar imaging has limitations that include uncorrected attenuation effects between the liver and lungs, lack of anatomical references for contouring, and a single standard lung mass value of 1 kg. These limitations combine to negatively affect the LSF calculations. In regards to SPECT/CT, a misregistration between the SPECT and CT data or truncated lungs due to a limited SPECT/CT field of view (FOV) will produce inaccurate LSF calculations.

3.7. Liver segmentation schemes

The Brisbane nomenclature is considered the standard liver segmentation scheme. Introduced and accepted by the International Hepato-Pancreato-Biliary Association (IHPBA), this standard was created to resolve the ambiguities presented by Couinard and Healey [30]. According to the Brisbane nomenclature, there are three orders of division based on the liver's internal anatomy: two hemilivers, sections or sectors, and segments [30]. The first-order division divides the left and right hemiliver by a plane called the midplane of the liver, commonly known as Cantlie's line. The second-order divisions divide the liver into smaller sections or sectors and have two distinct anatomical methods of dividing the liver. The liver sections are divided based on Healey's divisions, which are dependent on hepatic arteries and bile ducts. The liver sectors are based on Couinard's divisions, which are dependent on the portal veins. Both are considered correct divisions, but sections and sectors are not synonymous to each other and are considered distinct second-order divisions. In contrast, both third-order divisions are called segments based on Couinard's eight segments. Each of Couinard's segments is functionally independent and has its own vascular flow and biliary drainage [31].

In regards to radioembolization, Couinard's divisions are primarily used. The Couinard liver segmentation includes 'lobes', 'livers', 'sectors', and 'segments' [31]. In essence, the Couinard classifications are identical to Brisbane's standard, with the term 'livers' instead of 'hemilivers'. Furthermore, the surface anatomical method may be used to separate the liver into two lobes. The lobes are divided into the right and left lobes and are separated by the falciform ligament. The right lobe consists of segments 4–8 while the left lobe consists of segments 2 and 3. To note, most radioembolization literature references the differing treatment based on Couinard's "lobular" anatomy even though the Brisbane standard discourages its use [32–34].

3.8. Treatment

Radioembolization treatments are dependent on the tumour's location, number of tumours, arterial perfusion, and the liver's functional capacity. If a tumour is localized within a single liver segment and supplied by one main artery or arterial branch, super selective catherization or radiation segmentectomy is suggested. Radiation segmentectomy is when ^{90}Y based microspheres are infused within two or less hepatic segments [35]. This treatment administers high doses of radiation to the tumour and reduces the dose coverage to non-tumoural hepatic tissue. A less precise option, radiation lobectomy is an approach that treats either an entire right or left hepatic lobe. When surgical resection is not amenable or if the future liver remnant is deemed insufficient to sustain adequate hepatic function, radiation lobectomy is recommended. The effects of radiation lobectomy are two-fold; it aids in tumour control and produces contralateral lobe hypertrophy [32,34]. Contralateral lobe hypertrophy is an interesting result of radioembolization where the non-irradiated hepatic lobe increases in hepatic parenchyma size. Vouche et al. (2013) have postulated that radiation induced parenchymal lesions and a decreased blood supply shrinks the irradiated lobe and induces the portal flow to redirect towards the contralateral lobe [32]. This portal flow redirection induces the contralateral lobe to increase in size and, correspondingly, increase its functionality. Additionally, radiation lobectomy provides tumour control during the regenerative phase after treatment, providing a logical step before surgical resection [34].

The last radioembolization option is whole liver treatment and is required when many diffuse tumours are localized within both of the lobes. There are two methods of administering the same dose to the whole liver: sequentially through bi-lobar treatment or singularly through simultaneous treatment of both lobes. If treated sequentially, one lobe is treated first and after at least 30 days with sufficient liver regeneration the second lobe is treated [15]. When comparing the two, sequential radioembolization has resulted in fewer adverse side effects such as lower overall bilirubin levels and lower risks of developing radioembolization induced liver disease (REILD) [33]. Therefore, sequential liver treatment has become the more standard recommendation.

If feasible, more segmented therapy might be performed. If a singular artery branch is identified to perfuse the targeted tumour(s) then a more selective treatment can be used to infuse the microspheres. This serves to avoid extrahepatic deposition as well as to make treatment more spatially localized, providing higher dosages to the tumour and less intrahepatic radiation to the normal tissue. However, radioembolization is currently used as a primarily palliative treatment making more segmented treatments less likely and procedures such as sequential liver treatment the norm. Regardless, every ^{90}Y treatment should be delivered as selectively as possible to reduce irradiation of the normal liver parenchyma [5].

Further considerations are necessary to ensure an optimal or accurate radioembolization treatment. Lau et al. (2012) have provided ^{90}Y activity recommendations depending on the number of tumours, patient specifications, and type of treatment [12]. The same authors have also recommended threshold values to prevent REILD. Other considerations include similar catheter placement during ^{90}Y microsphere treatment as during Tc-MAA injections, otherwise up to 30% of differing activity may be measured and the resulting microsphere distribution may differ [37]. For SIR-spheres, a higher number of microspheres is injected to reach the same prescribed activity as each microsphere has less activity (50 Bq) compared to each Therasphere (2500 Bq) [2,5]. The greater number of SIR-spheres may cause an embolic effect called flow stasis, at which point microsphere administration should stop regardless of an incomplete administration of the total prescribed activity [8]. Since the initial prescribed calculations are based on the volume of the target, accurate volume measurements are necessary. Hepatic volume measurements should only include the tumour volume perfused by the targeted arteries [5,15]. The treatment itself should completely administer the dose throughout the whole tumour, which is achieved by injecting microspheres into all the arteries that perfuse the different parts of the tumours.

3.9. Current clinical dosimetric methods

When it comes to radioembolization's current clinical dosimetry, the ^{90}Y microspheres are calibrated, measured, and administered in activity (GBq). However, radiation therapy doses are normally planned in Gy (J/kg) to quantify absorbed dose from a radiation source in tissue. Likewise, radioembolization plans the prescribed doses to the patient in Gy, but converts it into prescribed activity before treatment.

The prescribed activity may not always be the activity that was administered. Differences between the prescribed and administered activity may exist due to an incomplete treatment. Aforementioned, SIR-spheres are known to have embolic tendencies that call for a halt in microsphere administration and may also have residual activity left after a complete treatment. Theraspheres may have approximately up to 5% of its residual activity left within the microsphere vial after every treatment [5,8]. The calculation of the administered activity is simply the residual activity or the activity left in the microsphere vial after treatment subtracted from the prescribed activity. The theoretical range of the residual activity is between zero and the prescribed activity.

More importantly, the absorbed dose should be corrected for the activity that was actually administered to the patent.

For absorbed dose calculations, radioembolization applies the MIRD formalism and directly translates activity in Bq to absorbed dose in Gy. For instance, the MIRD formula presented in Eq. (1) presents the simplest case where all the activity localizes within the volume of the perfused liver. Eq. (1) converts administered activity to absorbed dose by assuming that 1 GBq of administered activity per kg of tissue (liver) mass provides an absorbed dose of 49.38 ± 0.5 Gy, typically rounded up to 50 Gy. This is based on the assumption that ^{90}Y distributes uniformly within the tumourous tissue and healthy hepatic parenchyma to provide an evenly distributed absorbed dose.

$$\mathrm{D[Gy]} = 50\mathrm{[J/GBq]} \times \left(\frac{A\,[GBq]}{m\,[kg]}\right) \tag{1}$$

D[Gy] = Dose to Specified Liver Volume

In Eq. (1), A[GBq] represents the activity of ^{90}Y administered into the perfused liver while m[kg] represents the mass of the perfused liver. The derivation of this equation may be seen elsewhere [8,37]. A CT scan measures the liver volume that is then used to find its corresponding mass, which is achieved by multiplying the liver's density in g/cm^3 by its volume in cm^3 [37]. As discussed before (See 3.6 Lung Shunt Fraction), the administered activity may directly shunt to the lungs. This causes extrahepatic deposition and changes the absorbed dose distributed to the liver. If there is any lung shunting, the dose to the lung or liver may be calculated if the total activity is partitioned between the liver and lung volumes as seen in Eq. (3). Eq. (2), derived from Eq. (1), calculates the absorbed dose to the lungs and requires the tissue mass and partitioned activity of the lungs. Accordingly, the absorbed dose to the perfused liver is calculated given the mass and partitioned activity of the perfused liver. Illustrated later, this equation is seen in Eq. (14) and is also called the mono-compartmental method. Importantly, both dose estimations rely on the lung volume and the LSF, which is presented in Table 3.

$$\mathrm{D_{lung}[Gy]} = 50\ \mathrm{[J/GBq]} \times \left(\frac{A_{total}\,[GBq]}{m_{lung}\,[kg]}\right) \times LSF \tag{2}$$

D_{lung} = Dose to Lung

The corresponding activities in question may be calculated as seen in Eqs. (3)–(5). A_{liver} represents the partitioned activity within the perfused liver while A_{lung} represents the activity within the lungs.

$$\mathrm{A_{total}[GBq]} = \mathrm{A_{liver}} + \mathrm{A_{lung}} \tag{3}$$

$$\mathrm{A_{liver}} = \mathrm{A_{total}} \times (1 - \mathrm{LSF}) \tag{4}$$

$$\mathrm{A_{lung}} = \mathrm{A_{total}} \times \mathrm{LSF} \tag{5}$$

$\mathrm{A_{total}[GBq]}$ = Total Administered Activities

Table 3 presents the manufacturer's recommended lung shunt thresholds. Depicted in percentages or fractions, the recommendations provide no direct information on the threshold absorbed-doses to the lungs. However, both SIR-sphere and Therasphere threshold values are based on a maximum dose of 30 Gy for a lung mass of 1.0 kg [8]. These values were established because patients who received an estimated singular lung dose greater than 30 Gy and/or had a cumulative dose greater than 50 Gy for repeated treatments developed radiation pneumonitis [38,39]. It should be emphasized that these absorbed dose values were calculated from the LSF using planar imaging and the MIRD method of Eq. (2) [40]. Thus, patient eligibility was set at an upper threshold of 30 Gy under these specific conditions.

As previously discussed, the LSF may further be calculated by SPECT/CT images. Recently, Allred et al. (2018) demonstrated that planar imaging overestimated the LSF by up to 44% while SPECT/CT images showed a maximum deviation of 13% [27]. A poor correlation was further shown between LSFs calculated from planar and SPECT/CT imaging of Tc-MAA. Due to such poor correlations, the authors postulated that the previous thresholds of LSF, which were based on planar imaging, should be adjusted for those calculated by SPECT/CT [27,38,39]. Currently, all of the dosimetric equations use LSF in their calculations obtained through either planar or SPECT/CT imaging, but clinically planar imaging is more readily adopted.

In clinical practice, radioembolization dosimetry is calculated from different dosimetric equations to set the treatment prescribed dose as a prescribed activity. There are currently four different clinical dosimetric methods that are dependent on the type of microsphere. Three dosimetric methods are available if resin or SIR-microspheres are used. The first dosimetric method is the empiric method that bases its recommended activity on the percent tumour involvement on the whole liver. This method relies solely on CT or MRI images to determine the liver size and tumour burden percentage, but is now abandoned due to its low safety margins regarding radiation-induced side effects [12,13,41]. The empiric method shown in Table 4 prescribes an activity based on the tumour burden. When used in the past, the activity was reduced based on the LSF.

Formulated after the empiric formula, the body surface area (BSA) is the most commonly used method due to its simplicity and ease of use. This method assumes that the size of the patient's whole liver correlates with the patient's BSA [42]. Thus, a prescribed activity could appropriately be adjusted to a patient's malignant liver volume without the need for liver volumetry on cross-sectional imaging [41]. Similarly to the empiric method, the BSA could also take into account the LSF to reduce unwanted radiation within the lungs (Table 4). The activity prescribed is calculated as described in Eqs. (6) and (7):

$$\mathrm{A[GBq]} = (\mathrm{BSA} - 0.2) + \left(\frac{tumour\ volume}{tumour\ volume + liver\ volume}\right) \tag{6}$$

$$\mathrm{BSA} = 0.20247 \times \mathrm{height[m]}^{0.725} \times \mathrm{weight[kg]}^{0.425} \tag{7}$$

In Eq. (6), A[GBq] stands for prescribed activity and the tumour and liver volumes may be analyzed from the patient's CT or MRI scans. With

Table 3
Description for Calculation of LSF.

LSF Calculation	$\mathrm{LSF} = \frac{counts_{lung}}{counts_{lung} + counts_{liver}} \times 100$ for lung shunt percentage	
SIR-Sphere (Resin) [4]	LSF	Activity Given
	> 20%	No Activity
	15%–20%	Reduce by 40%
	10%–15%	Reduce by 20%
	< 10%	Give full amount of activity
TheraSphere (Glass) [3]	Upper Lung Shunt Activity Limit: LSF [%] × A[GBq] = 0.61 GBq A[GBq] = Activity prescribed during pre-treatment dosimetry	

These calculations are recommended based on planar scintigraphic imaging, but SPECT/CT derived data is much more reliable.

Table 4
Prescribed Dose Based on Tumour Load.

Resin		Reduced Load for Resin based on Lung Shunt	
		Lung Shunt Percentage	Activity of Spheres
Empiric Method	> 50% Tumour Load = 3 GBq	< 10%	Full prescribed activity
	25–50% Tumour Load = 2.5 GBq	10–15%	Reduce activity by 20%
	< 25% Tumour Load = 2 GBq	15–20%	Reduce activity by 40%
		> 20%	Do not give SIR-Spheres

no explicit method given, the absorbed dose calculations should use the MIRD equations (Eqs. (1), (2), (14)). It is important to note, however, that the BSA prescribed activity and the absorbed dose to the whole liver were found to be poorly correlated to one another and had a 2.5 fold difference [43,44]. It was found that larger livers were relatively underdosed while smaller livers were overdosed with the BSA method. Other limitations to the BSA equation include a disregard to the tumour-to-normal liver ratio (T/N) and establishment of an artificial limit to the injected ^{90}Y activity from 1 to 3 GBq [45]. To clarify, the T/N ratio is a compartmental or tumour-specific ratio that measures the relative difference of microsphere deposition between the tumourous and non-tumourous tissue per unit mass. This ratio is estimated from the Tc-MAA image as the activity of the tumour (A_{tumour}) and normal liver ($A_{normal\ liver}$) in counts are divided by the mass of the tumour (m_{tumour}) and normal liver ($m_{normal\ liver}$) in kg. The T/N ratio ends up unitless and is demonstrated in Eq. (8):

$$\text{T/N Ratio from Tc−MAA Image} = \frac{A_{tumour}/m_{tumour}}{A_{normal\ liver}/m_{normal\ liver}} \tag{8}$$

The most accurate of these three SIR-sphere dosimetric equations is called the partition method or model and is the only SIR dosimetric equation formulated directly from the MIRD methodology. In essence, the partition method partitions the previously described perfused liver into tumourous and non-tumourous (normal liver) volumes and includes the lungs, resulting in three separate compartments for dosimetry [38,46]. Taking into account the T/N ratio, the LSF, and the masses of the normal liver (m_{normal}) and tumours (m_{tumour}), the partition method is the most patient-specific method of the three SIR-sphere equations [47]. With CT/MRI partitioned masses, the partition method preserves the dosimetric viability that may have been lost due to any volumetric liver changes caused by previous treatments (e.g. surgery). The lung partition is normally determined through the calculation of the LSF (Table 3) with Tc-MAA planar imaging or SPECT/CT. LSF inclusion provides a more representative proportion of administered activity that the total perfused liver may receive. The Tc-MAA image is additionally used to calculate the T/N ratio (Eq. (8)). This ratio allows the partition method to prescribe an activity that is limited by the maximum dose acceptable to the normal liver and is seen below:

$$\text{A[GBq]} = \frac{D[Gy] \times \left(\frac{T}{N} \times m_{tumour}[\text{kg}] + m_{normal}[kg]\right)}{50\ [J/GBq] \times (1 - LSF)} \tag{9}$$

D[Gy] = Maximum Dose for Perfused Normal Liver

A[GBq] = Total Prescribed Activity

Depending on whether or not SIR-spheres have been administered, the absorbed dose to the different partitioned volumes may be calculated from the prescribed or administrated activity. Stemming directly from the MIRD method, the absorbed dose to the normal liver (D_{normal}) and tumour (D_{tumour}), takes the MIRD formula (Eq. (1)), and accounts for the liver partitions to produce Eqs. (10) and (11) [8]. A_{normal}, A_{tumour}, and A_{lung} represents the respectively partitioned activities within the normal liver, tumourous liver, and lungs. The absorbed dose to the lung is calculated in the same way as in Eq. (2) while the A_{lung} is calculated as in Eq. (5). To find the A_{normal} and A_{tumour}, the Tc-MAA counts within the tumour and normal liver regions of interest (ROIs) are divided to find a counts ratio. Counts are assumed to be proportional to activity, hence the count ratio is equivalent to the activity ratio. Not to be confused with the T/N ratio, this activity ratio along with a calculated A_{lung} is input into Eq. (12) to find the resulting A_{normal} and A_{tumour} activities.

$$D_{normal}[\text{Gy}] = \frac{50\ [\text{J/GBq}] \times\ (A_{total})[GBq](1 - LSF)}{m_{normal}[\text{kg}] + T/N\,(m_{tumour})[\text{kg}]} \tag{10}$$

$$D_{tumour}[\text{Gy}] = \text{T/ N}\times D_{normal} \tag{11}$$

$$A_{total} = A_{normal} + A_{tumour} + A_{lung} \tag{12}$$

A_{total} = Total Administered Activity

While the partition method is the most accurate among the current clinical dosimetric methods, this method still has many limitations. Logistics of the partition model may require a strong working relationship between the nuclear medicine physician and the interventional radiologist; otherwise, the nuclear medicine physician may not be properly informed about the heterogeneities within the vasculature and the appropriate delineations of the ROIs [45]. Furthermore, the partition method is based on the assumption that correct ROIs were drawn on the image. Depending on the institution, physician, tumour characteristics, and the resolution of the image, the ROIs may vary or be inaccurate. The ROIs considered are the partitioned volumes: tumour within the liver, normal liver, and lung. Tumours that are well defined and large such as hepatocellular carcinomas (HCC) are commonly prescribed doses with the partition method because of their clear ROIs. However, if ROIs cannot be well defined and partitioned, then the partition method cannot be accurately used. In addition, the T/N ratio lacks a standardized methodology, which leads to further variability in dosimetric reports [48].

Compared to SIR-microspheres, the glass microspheres or Therapheres have only one dosimetric method known as the mono-compartmental method [3,37]. When calculating the prescribed activity (Eq. (13)), the assumption that 1 GBq of administered activity per kg of tissue mass equates to 50 Gy is inherently factored in. In contrast to the partition method, the mono-compartmental method only takes into account the total perfused liver volume without partitioning the liver into more discrete and separate units (Eqs. (9)–(12)). This simplification makes the absorbed dose calculations less spatially precise and accurate. When activity is converted to absorbed dose, LSF is taken into account as to not over-estimate the resulting absorbed dose. In other words, the prescribed absorbed dose solely considers the administered activity localized within the liver as a whole.

$$\text{A[GBq]} = \frac{\text{D[Gy]} \times m_{liver}[\text{kg}]}{50[\text{J/GBq}] \times (1 - LSF)} \tag{13}$$

D[Gy] = Prescribed Dose for Perfused Liver

Described previously, the Therasphere absorbed dose is derived from MIRD and is calculated by partitioning the liver and the lungs (Eq. (2)–(5)). In parallel with SIR-spheres, this method takes into account either the prescribed or administered activity and is seen here:

$$\mathrm{D[Gy]} = \frac{50\ [\mathrm{J/GBq}] \times A\ [GBq\ of\ Administered\ Activity] \times (1 - LSF)}{m_{liver}\ [\mathrm{kg}]} \quad (14)$$

D[Gy] = Administered Dose to Perfused Liver

It is worth noting that both SIR-spheres and Theraspheres have clinical dosimetric methods that are derived from the same MIRD formalisms (Eq. (1)). In this regard, radioembolization treatments with SIR-sphere may apply the mono-compartmental method. More notably, Therasphere treatments may apply the SIR-sphere partition method for more accurate clinical dosimetry.

3.10. Shared limitations in the current clinical dosimetric methods

There are a few shared limitations within all the current clinical dosimetric methods. Mainly, the microspheres are not uniformly distributed within the treated liver. As will be subsequently discussed, the microsphere distribution is highly heterogeneous within both tumour and non-tumourous hepatic tissue. Consequently, radioembolization dosimetry is best modelled as heterogeneous clusters of point-sources that emit beta irradiation [45]. With current methods, the spatial distribution of a microsphere's absorbed dose is ignored [12]. Rather, an absorbed dose is attributed to an entire region. For instance, the partition method accounts for the T/N ratio, which calculates the ratio of microsphere distribution between the tumourous and non-tumourous ROIs. Assume a simple scenario where one tumour exists and the partitioned absorbed dose to that tumourous region is calculated to be 120 Gy. In this case, the tumour ROI is said to receive a uniform dose of 120 Gy, but due to a heterogeneous microsphere distribution that depends on the micro-vasculature, the real dose distribution will be variable throughout. Only specific portions of the ROI may actually receive 120 Gy. Thus, a microsphere's micro-distribution will greatly affect where the dose is deposited.

Additionally, the long beta particle range for ^{90}Y microspheres is neglected within these methods. This limitation becomes the most apparent with the partition method when the liver is divided among the tumourous and non-tumourous regions and is in close proximity to each other. Here, the ^{90}Y beta particles are arbitrarily delimited within a specific region (e.g. tumourous) and it is assumed that the entire dose is deposited within. However, the beta particles emitted from ^{90}Y may cross into and deposit their dose in the non-tumourous region. This phenomenon, when a non-targeted region obtains a dose of radiation from a neighbouring targeted region is called the "crossfire" effect. The partition method was determined as inaccurate due to the exclusion of the crossfire effect within a MIRD-5 human phantom [49]. This inaccuracy was illustrated more remarkably between the tumourous and non-tumourous region when the T/N ratio and tumour involvement was high while the LSF was less than 10%. Furthermore, the dose to the liver may be underestimated within the lung boundaries due to the long range of beta particles emitted from ^{90}Y. This concept may be applied to the rest of the current clinical dosimetry methods when ^{90}Y microspheres are located at the edge of the delimited regions of the lung or liver. As a result, the beta particles emitted from ^{90}Y decay may escape and provide a lower absorbed dose than prescribed in the specific ROI.

3.11. Liver microcirculation & distribution

Although the knowledge of the macroscopic hepatic vasculature is enough for radioembolization treatment, dosimetry depends on the microspheres' physical distribution within the hepatic microcirculation. Starting from the left or right hepatic arteries, hepatic microcirculation starts when these arteries divide into smaller arterioles (diameter 50–100 μm), terminal arterioles (diameters 15–50 μm), and reach the true capillary network (diameters 5–10 μm) otherwise called the sinusoids within the liver [17,50]. With diameters of SIR-spheres or Theraspheres spanning only 20–30 or 20–60 μm, respectively, the microspheres should localize uniformly within the terminal arterioles of both the normal and tumour tissue. As was described earlier, many dose calculation formalisms base their methods after a uniform microsphere distribution within the liver. But in fact, multiple studies illustrate heterogeneous microsphere deposition. Fox et al. (1991) first described the inhomogeneity with SIR-spheres by taking two tissue samples of approximately 1 cm^3 from a representative area of normal liver tissue that had been treated [51]. The authors showed that compared to the assumed uniform distribution, 86.2% of the normal tissue received less than the expected dose from a uniform distribution and up to 33.7% of the same tissue received less than one-third of this lower than expected dose. In another study, by sectioning a 10 mm piece of a resected lobe that was treated with $6x10^7$ spheres (3.2 GBq), Campbell et al. (2000) similarly showed that normal tissue had a non-uniform distribution of microspheres [52]. Hence, the absorbed dose in normal tissues was heterogeneous rather than homogenous. Within tumour tissue, the same authors illustrated that the microspheres deposited predominantly on the periphery of the tumour and clustered together. The microspheres were likely (90%) to cluster in groups of up to 65 microspheres with cluster sizes varying from 20 to 1500 μm in diameter. Based on Campbell's data and a basic dosimetric model, it was found that an average of > 200 Gy was deposited within 6 mm of the tumour and 2 mm into the normal tissue when measured from the tumour-normal tissue boundary [53]. Clustering of the microspheres caused an absorbed dose above average within the clusters while the absorbed dose decreased with distance from the cluster. With most of the ^{90}Y microsphere absorbed dose deposited near its source, it was shown that less than 1% of normal tissue received greater than 30 Gy. For large tumours, only the periphery would obtain a large absorbed dose.

Although these previous studies discussed SIR-spheres, it was demonstrated through four whole explanted livers that both SIR- and Theraspheres dispersed similarly within the edge of the tumour nodules [2]. With the exception of one patient, microspheres were deposited preferentially with a ratio from 2:1 to 16:1 within the tumour periphery compared to the non-neoplastic tissue. Additionally, the authors found most of the microspheres in groups of 1 to 4, where nearly all microspheres were found lodged in the periphery of the triad units within the small and terminal arterioles (12–30 μm). Dosimetrically, the cluster had an absorbed dose cloud of 300 Gy and rapidly fell in absorbed dose to 100 Gy within 4 mm.

More recently, a statistical study showed that within one patient's normal liver parenchyma the coefficient of variation (CV) of the activity concentration distribution in biopsies decreased with an increasing biopsy volume size, illustrating that the heterogeneity of microsphere deposition wasn't limited microscopically, but also relevant macroscopically to the whole liver [54]. Through the same patient's distribution analysis of 250 sections, the same authors elaborated on the cause of whole liver non-uniformity [55]. The authors found a linear increase in mean number of spheres per section with cluster size. Clusters of microspheres were aggregated within small arteries where small arteries were upstream of normal and terminal arterioles. As microspheres clustered within small arteries, systematic structural non-uniformity developed due to these clusters inhibiting the flow of microspheres into the smaller arterioles. Accordingly, the authors concluded that a larger number of spheres injected would result in larger dose inhomogeneity.

With these studies, modified recommendations may arise in regards to the current methodologies of clinical practice. Repeated radioembolization treatments could become standard procedure to fully treat larger tumours. Higher threshold for administered dose based on current clinical dosimetric methods could be set. This higher threshold administration may promote a more effective treatment due to a higher absorbed dose while minimally irradiating the normal hepatic parenchyma, which receives a fraction of the dose due to non-homogenous microsphere distributions [5,51,52,55–57]. Dosimetry implications

arise as well. Radiobiological and dosimetrical effects would need to consider the effects of microsphere heterogeneous deposition. Dosimetry would further be affected by the microanatomy of a patient's liver, crossfire effects at the cellular level, microsphere bifurcation effects within hepatic arteries, and the differences in therapeutic effect when different microsphere numbers and sizes are injected within a patient. These issues are explored elsewhere [58–61].

3.12. Post-treatment imaging and its applications

Radioembolization post-imaging provides a means to document the true microsphere distribution, estimate activity in the tissue, validate predictive doses of microsphere radiation, and visualize their final bio-distribution. With the advent of quantitative SPECT (QSPECT) and PET scans, ^{90}Y has had two principle modalities of acquiring quantitative images. It is more common for patients to be imaged by SPECT than PET; however, SPECT has more limitations. ^{90}Y is a pure beta-emitter that produces mostly bremsstrahlung photons with an energy spectrum up to the maximum energy of the beta particles, i.e. 2.27 MeV. The energy spectrum of photons emerging from the patient and measured by a photon detector has no photopeak, hence, it is difficult to select a proper energy window. Photons will also attenuate while interacting with the patient's tissue and may undergo the photoelectric effect, coherent scattering, and Compton scattering that cause photons to lose their original direction. In addition, the detectors used in SPECT are designed to detect photons emitted by the conventional diagnostic radionuclides, which have lower energies. The photons belonging to the highest energy region of the ^{90}Y bremsstrahlung photons may pass through the collimator septa or scatter in, lowering the image quality [62]. In fact, all raw SPECT images intrinsically contain such limitations; however, corrections can be applied during the reconstruction process. Depending on a reconstruction algorithm's corrections, SPECT images may be considered quantitative to a varying degree [63]. Presently, a number of specific modeling techniques and corrections have been developed to improve the image quality of SPECT and produce good image quantification. Without these corrections, for instance for scattered photons, the resulting image would lose image contrast and present poor quantification [63]. Co-registered CT data with SPECT allows some attenuation and scatter corrections. A proper energy window optimizes the signal to noise ratio (SNR) for photons [64,65]. More advanced algorithms can help with the image formation process that improves on attenuation, scatter and the use of a proper collimator may help with reduced photon penetration [63,66–69]. Unfortunately, QSPECT algorithms are neither readily available nor normally implemented clinically. Fig. 3 demonstrates an example of a post-treatment SPECT/CT image set. Hereafter, all references to SPECT/CT within this manuscript may be assumed to be quantitative (QSPECT/CT) in nature.

In contrast, PET has always been known as a quantitative imaging modality that provides higher quantification due to its superior spatial resolution and sensitivity. The decay of ^{90}Y has a minor branch to the 0^+ excited state, creating a positron and electron pair every 32 in one million decays. The annihilation of this positron is used in PET imaging for radioembolization quantification [70]. It has been shown that time-of-flight (TOF) PET and standard PET scans can both illustrate the localization and bio-distribution of ^{90}Y. TOF PET provides further advantages over standard PET by providing a gain in image SNR, improved lesion detectability, and uptake measurements [66,71]. PET with a co-registered CT (PET/CT) additionally provides attenuation corrections [66]. Furthermore, image reconstruction algorithms and optimized PET/CT settings have allowed for accurate ^{90}Y-based radioembolization quantifications. A multi-center study has provided a comparison between the different vendor PET/CT detectors and their quantitative results of ^{90}Y imaging [72].

With two imaging modalities for ^{90}Y-based radioembolization, the quantitative comparisons between SPECT/CT and PET/CT have been investigated with ^{90}Y microspheres. Yue et al. (2016) compared the activity differences between SPECT with a multiple energy range (MER) reconstruction technique and non-TOF PET without random correction based on prompt coincidences [73]. The MER reconstruction technique included Monte Carlo (MC) simulations that accounted for geometric sensitivities, collimator-detector responses, and scatter kernels. The authors reported great agreement between the two imaging modalities with overall liver activities within 11% for 12 of 15 patients. At a voxel level, excellent quantitative agreement between PET and SPECT images were illustrated. However, the reconstructed voxels between SPECT and PET with low or no activities had a significant difference. More specifically, it was observed that PET overestimated the ^{90}Y in low or no activity regions. Nevertheless, the authors concluded that SPECT and non-TOF PET images were in good agreement because most general deviations could be attributed to image noise. Elschot et al. (2013) compared the latest TOF PET/CT with SPECT/CT images and showed that with equal noise TOF PET/CT had a higher contrast recovery coefficient than SPECT/CT [74]. The authors showed consistent data demonstrating that SPECT/CT and PET/CT were both able to visualize extra- and intra-hepatic microsphere depositions [74]. They went further to state that PET scans were able to uniquely detect smaller accumulations of activity than SPECT. Similarly, another TOF PET and SPECT comparison was performed. Here, the authors illustrated TOF PET's superiority and concluded that PET/CT outperformed SPECT/CT in resolution, detection in non-target activity, and provided better information of ^{90}Y activity within regions of targeted tumour vascular thrombosis [75]. However, this imaging modality study was more qualitative than quantitative in nature.

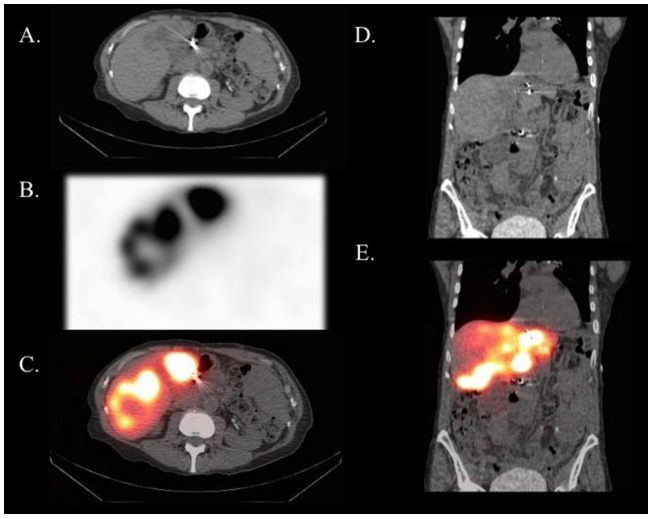

Fig. 3. This figure represents a post-treatment SPECT/CT image for a radioembolization patient. Part A illustrates a standard reconstructed CT image while Part B illustrates a reconstructed SPECT intensity image. A fused image can be seen in Part C where the activity distribution of SPECT is anatomically localized in the liver CT. Part D is the same Part A image shown in a coronal slice. Furthermore, Part E is same fused image of Part C shown in the coronal slice.

Depending on the reconstruction algorithms, SPECT and PET scans may produce similar or differing reconstructed images. For example, Elschot et al. (2013) had all the PET algorithms corrected for scatter, attenuation, random coincidences, point spread function (PSF), and had TOF information while the SPECT reconstruction algorithms only corrected for attenuation and PSF (collimator-detection) [74]. Likewise, Kao et al. (2013) compared TOF PET/CT, which had a 3D-iterative ordered subset expectation maximum (OSEM) algorithm correcting for attenuation, scatter, random coincidence, dead time, and normalization, with SPECT/CT reconstructed with a 3D-OSEM algorithm that corrected for attenuation [75]. Therefore, these studies may have biased TOF PET performance based on image reconstruction algorithms alone. In contrast, Yue et al. (2016) corrected for photon scatter, attenuation, and collimator detection in both imaging modalities and were able to show a more comparable analysis to non-TOF PET and

SPECT scans [73]. Nevertheless, TOF PET scans seems to predominate in quantitative analysis by providing a more precise and accurate detection through a higher SNR and providing an intrinsic correction factor for count attenuation and intensity [63,74,75].

3.13. Image based dosimetry and its limitations

Image based dosimetry uses SPECT/CT and PET/CT images to calculate a more accurate dose based on pre-treatment or post-treatment images. A review has summarized (3D) image based dosimetry into the general methodologies that constitutes local deposition methods, dose-kernel convolutions, and MC simulations [76]. Dezarn et al. (2011) further recommend how to proceed on calculating doses at the voxel-level [8]. While consistently investigated, image based dosimetry recommendations have yet to solidify a standardized consensus on the methodology of calculating image-based doses.

Compared to the current clinical dosimetric methods (See 3.9 Current Clinical Dosimetric Methods), image based dosimetry relies more directly on SPECT/CT or PET/CT images obtained from the pre-treatment or post-treatment imaging steps. Independent of tumour burden, tumour segmentation, or tumour uptake fractions, image based dosimetry estimations rely mainly on image quality such as image resolution and reconstruction parameters [77]. Moreover, image based dosimetry makes fewer assumptions than the current clinical dosimetric methods. In the case of direct-transport MC simulations, factors such as tissue heterogeneity, crossfire effects, and non-uniform distributions can all be accounted for. Depending on the implementation, individual particles are simulated based on verified cross-sectional probabilities. Any significant particle interaction is then explored within a user-defined world and permits accurate dose calculations to the size of any given image voxel. To note, tumour and organ contouring are still necessary, but are not a requisite for voxelized dose calculations. For instance, the voxel doses based on post-treatment PET/CT voxel-based dosimetry would stay constant while the reported absorbed doses within a ROI contour may change depending on the physician's contour drawing methodology, subsequently, making image-based dosimetry a great utility for retrospective analysis.

Nevertheless, image-based methods should not be construed as without dosimetric limitations. Currently, the spatial resolution of our imaging systems cannot resolve the microsphere microscopic spatial distribution. For radioembolization, a microsphere may range from 20 to 60 μm in diameter. A CT voxel may be sub-millimeter in the x and y dimensions, but PET and to a larger regard SPECT voxels both fall closer to the multi-millimeter than sub-millimeter range. Resolution of a SPECT or PET voxel, which contains the microsphere's spatial locations, is poor when compared to a single microsphere's diameter. This will spatially limit accurate absorbed dose calculation methods such as the MC method. The problem is due to the fact that objects approximately three times less than the imaging modality's full width half max (FWHM) lead to loss of information and an underestimation of count data [63]. Poor resolution may also affect image based dosimetry methods differently. Indeed, high correlations were illustrated when absorbed dose in tumours and normal liver was compared between the partition method and dose-kernel convolution method [78]. Poor resolution may have clustered the microsphere's activities and resulted in seemingly uniform absorbed dose similar to those of the partition method. However, a MC comparison study showed much lower correlation within tumour voxels, while significant differences were observed between absorbed dose claculated with MC and current clinical dosimetric methods [48]. This result may indicate that poor imaging resolution has less of an effect on MC dosimetry due to more accurate simulatation of radiation interaction with matter. It could be argued that heterogeneous tissues may have played a role in the MC simulations; however, dose-kernel convolutions were based off S values that accounted for soft tissues similar to that of the MC simulations, which makes tissue heterogeneity a less likely dosimetric factor [48,79]. Most importantly, image-based dosimetry relies on the data of a reconstructed image, which is reliant on the accuracy of the image reconstruction method used. An entire field in itself, it is essential to briefly note that the accuracy and precision of an image reconstruction method becomes the core limitations to all image-based dosimetric analyses. In other words, the myriad of physics and hardware limitations that are relevant to a reconstruction process are relevant to the image-based dosimetry process as well: energy window choice, collimator choice, detector specifications, and reconstruction algorithms. A dosimetric method is only as accurate as the factors that helped reconstruct the image. Despite these limitations, however, image based dosimetry is already an improvement to the current quality of dosimetry methods. An emerging dosimetric methodology, image based dosimetry will likely improve over time.

3.14. Tc-MAA dosimetry

Tc-MAA injection, imaging, and results have an important diagnostic role within the radioembolization treatment. The recommendation of using Tc-MAA SPECT/CT imaging for patient based dosimetry has paved the way for investigating more accurate predictive dosimetry and the evaluation of dose to tumour responses [25,80]. Still, the efficacy of predictive dosimetry of Tc-MAA and its dose to tumour responses are debated. To start, Tc-MAA compared to ^{90}Y microspheres are inherently different in size, radioactivity, number, and density [19]. Based on what is called the skimming effect and axial accumulation, large Tc-MAA particles could preferentially deposit in vessels of high flow while smaller particles are diverted to vessels with lower flow [19]. In other words, the larger variability in Tc-MAA's size would result in a higher heterogeneity of Tc-MAA distribution compared to those of the ^{90}Y microspheres. In addition, Wondergem et al. (2013) showed that Tc-MAA poorly predicts intrahepatic distribution of ^{90}Y SIR-spheres by studying 225 volumes of interest (VOIs) delineated from Tc-MAA SPECT/CT and ^{90}Y PET/CT images of 31 patients [36]. Comparing SPECT/CT to PET/CT images, a difference of > 10%, 20%, and 30% were seen for 68%, 43%, and 32% of the 225 VOIs segments within a 95% confidence interval, respectively. The authors also found that compared to an optional catheter tip position, a suboptimal tip position could attribute to a higher percentage of differences between the Tc-MAA SPECT/CT images and the ^{90}Y PET/CT images. Interestingly, Kao (2013) in a letter to the editor explained that the 95% agreement was too stringent a threshold for clinical implications [81]. Kao suggested that one standard deviation or a 68% agreement would suffice. In their reply to Kao, Lam et al. (2013) agreed albeit with qualifications [82]. First, they agreed that Tc-MAA should still be clinically utilized as long as Tc-MAA and ^{90}Y distribution differences would improve over time, but qualified that the Tc-MAA predictive distribution should be used cautiously until then. In another study, Ulrich et al. (2013) evaluated treatment response and lesion size from Tc-MAA uptake and catheter placement in 435 colorectal metastasized tumours from 66 patients [83]. Tc-MAA uptake, catheter placement, nor their interaction effects were deemed significant to treatment response based on response evaluation criteria in solid tumours (RECIST) criteria. RECIST provides a standardized set of response on tumour shrinkage based on MRI or CT images. The criterion divides tumour shrinkage into four sections: complete and partial shrinkage, stable disease, or progressive disease [84]. However, the results from Ulrich et al. (2013) were critiqued for their poor methodology where subjective image-based Tc-MAA uptake was used to quantify dosage without any dosimetry calculations [83,85,86].

Other studies have contradicted the poor predictive results of Tc-MAA. In one study, Tc-MAA predictive dosimetry was demonstrated to strongly correlate with patient responses [87]. Here, a more optimistic progression-free survival (PFS) and overall survival (OS) within the European association for study of the liver (EASL) criteria was correlated for absorbed doses to tumours > 205 Gy while absorbed doses less than 205 Gy was correlated to a worse prognosis. In fact, the authors increased the prescribed activity among four patients to obtain an absorbed dose above 205 Gy that resulted in three patients responding to treatment. To note, the EASL criteria provides clinical practice guidelines and standards to diagnose, treat, and prevent liver diseases such as for HCC tumours. A more recent study had a uniform and repeatable radioembolization treatment [88]. Using the same staff, which led to homogeneity of patient

preparation, activity administration, imaging procedure, and data analysis, the authors compared both SIR-spheres and Theraspheres to Tc-MAA predictive dosimetry and illustrated that Tc-MAA and SIR-sphere dosimetry agreed overall. When comparing tumour mean doses between pre-treatment and post-treatment results Tc-MAA doses were more comparable to SIR-spheres (lin concordance, r = 0.69), than to Theraspheres (r = 0.44). Exploring the Tc-MAA predictive compatibilities with SIR-spheres, authors found that tumours > 150 ml were more comparable (r = 0.93 for Dmean). Within non-tumour liver tissue, both SIR-spheres (r = 0.93) and TheraSpheres (r = 0.99) had much better mean dose correlations to Tc-MAA. Thus, non-tumour liver tissue had a lower variability between predictive and post-treatment dosimetry leading to the conclusion that over-dosing to normal liver parenchyma can be avoided with pre-treatment Tc-MAA injections. Similarly, Song et al. (2015) illustrated an overall and significant correlation between Tc-MAA SPECT/CT pre-treatment and ^{90}Y PET/CT treatment dosimetry [89]. However, the individual differences between LSF, absorbed dose to the tumour, and absorbed dose to the lungs were also deemed significant. Tc-MAA pre-treatment dosimetry led to an over-estimated LSF and an underestimated absorbed dose to the tumour and non-tumour liver tissues. Additionally, significant correlation was seen between post-treatment PET/CT dosimetry and PFS when the tumour absorbed over 200 Gy. However, for these patients the statistical analysis of the pre-treatment Tc-MAA was unavailable to make a dose to tumour comparison. Nevertheless, the authors deemed Tc-MAA a useful clinical tool for conservative dosimetric estimates for radioembolization.

3.15. Post-treatment image based dosimetry

After ^{90}Y treatment, post-treatment image based dosimetry may be used to retrospectively quantify the absorbed dose of an administered treatment. Studies focusing on post-treatment image based dosimetry are listed in Table 5. Using PET/CT, D'Arienzo et al. (2012) conducted a voxel-based dosimetry study based on convolved S values, MC simulations, and a MATLAB software [90]. After verifying the software with phantom measurements, a subsequent and retrospective study was performed on one patient with metastatic colorectal cancer treated with ^{90}Y-based radioembolization [91]. The authors divided the tumour ROIs into two tumourous regions, tumours with a necrotic core and those without. Calculating the dose volume histograms in both regions, the authors found that necrotic core tumours received an average dose of 71.6 Gy that was correlated with progressive disease. Within the other treated tumourous area, a complete response was documented with an average of 286.9 Gy estimated over the whole region. Within 23 patients, Kao et al. (2013) utilized a simplified dosimetric approach by calculating voxel mean and self-defined radioconcentrations rather than implementing an image-based methodology on post-treatment radioembolization PET/CT images [92]. Only 8 patients were further studied due to strict tumour criteria and of those chosen, their tumour responses were reported using the mRECIST criteria. These patients had varying tumours that included HCC, cholangiocarcinoma, and adrenal metastatic gastrointestinal stromal tumours. To clarify, the mRECIST criterion is a modified RECIST criterion that is specific to HCC tumours and only takes into account the viable portions of lesions to assess treatment efficacies [84]. Defining D_{70} as the minimum dose received by 70% of the tumour and V_{100} defined as the percent of the target volume receiving 100% of the prescribed dose, the authors found that tumours receiving D_{70} over 100 Gy had a complete response while tumour receiving D_{70} under 100 Gy had an incomplete response. In another study, a modified local deposition model was applied to a cohort of 56 HCC patients representing 98 tumours [93]. A delivered dose ranging between 0 and 570 Gy with a mean absorbed dose of 169 Gy was observed. The authors came to the conclusion that the prescribed dose should be > 100 Gy and observed that the majority of tumours receiving such an absorbed dose were less than 100 ml in volume. The authors then assessed 48 acceptable tumours and compared them through the mRECIST criteria. There was no

Table 5
^{90}Y Post-treatment Image Based Dosimetry Studies.

Study	Imaging Modalities	Dosimetry Calculation Method	Tumour Response Criteria/ Microsphere Type(s)	Tumour Response by Dose (Gy)
[94]	SPECT/CT	MC voxel dose-kernel based on water	RECIST and EASL SIR-spheres	73 Patients EASL • D_{avg} 120 Gy, D_{med} 111 for CR RECIST • D_{avg} 122 Gy, D_{med} 99 for CR
[90,91]*	PET/CT	MCNPX based voxel dose-kernel convolution method with S values	18-FDG PET/CT and CT follow up at 6 months SIR-spheres	One Patient • Tumour Progression at avg. 71.6 Gy • Complete Remission at avg. 286.9 Gy
[92]	TOF PET/CT	Voxel mean radioconcentrations	mRECIST SIR-spheres	23 Patients • D_{70} > 100 complete response • D_{70} less than 100 Partial response or no response • Smaller tumour reached D_{70} > 100 easier
[93]	PET/CT	MIM software and modified local deposition model	mRECISTTherasphere	98 Tumours, 56 Patients • Not significant data • Theorize > 150 Gy for SD and > 200 for a response
[95]	PET/CT	Dose-Volume Kernel Method	mRECIST Therasphere	27 Patients and 38 Tumours** • D_{70} Responders = 140 Gy (28–450 Gy) vs. D_{70} Non-Responders = 24 Gy (10–133 Gy) • Responders Median = 225 Gy (51–631) vs. Non-Responders Median = 82.7 (48–199)
[96]	SPECT/CT	^{90}Y SurePlan; local-deposition method	mRECIST (ˆRECIST WHO) Therasphere	34 Patients with 53 tumours (max 3 per patient) • ˆWHO and RECIST showed no significance for voxel-dose and BED values*** • D_{mean} for mRECIST criteria was 263 Gy for responders and 147 Gy for non-responders • mRECIST Criteria at $D_{50\%}$ showed a mean of 160 Gy and 95% CI between 123 and 196 Gy. • No significant correlation between D_{mean} or V_{30Gy} (Volume that receives at least 30 Gy) with toxicities

* Focuses on the dosimetry of the 2013 study, but methodology is located within the 2012 study.
** Values are of Tumour dose.
*** Bed Values are not reported because they were not explained within the review.

statistical significance between absorbed dose and tumour response and therefore only a suggestive trend of tumour response to high-absorbed dose could be concluded. However, the authors noted that the absorbed doses in normal liver gave a significant correlation between the absorbed dose and two or more severe liver complications. The authors concluded that with every 10 Gy increase in the normal liver parenchyma, an estimated 61% increase in the odds of liver complications would ensue. Strigari et al. (2010) further calculated the absorbed dose through SPET/CT with dose-kernel calculations based on MC simulations in water [94]. Reporting a mean dose of 110 Gy to the target volume for 73 patients with HCC, the authors illustrated a complete or partial response for 74% of the tumours using the EASL criteria and a complete or partial response for 55% of the tumours using the RECIST criteria. With normal liver tissue, a median of 36 Gy was seen to cause grade 2 to 4 toxicities in a portion of the treated patients. Other authors have analyzed 27 patients and performed a per lesion analysis on 38 HCC tumours [95]. Characterizing patient responses based on the mRECIST criteria, two patient groups were analyzed including a responder (Complete and Partial Response) and non-responder group (Stable Disease and Progressive Disease). The authors demonstrated that the non-responders had an absorbed dose median of 83 Gy while the responders had an absorbed dose median of 225 Gy and further reported that an absorbed tumour dose threshold of 200 Gy could predict a HCC response with 66% sensitivity. In another dosimetric study, the ^{90}Y SurePlan commercial software by MIM [96] was used to perform post-treatment dosimetry on 34 patients with HCC. A total of 53 tumours were analysed with no more greater than three tumours taken from each patient. Utilizing the mRECIST criteria in this study, the logistical regression analysis demonstrated that the $D_{50\%}$ (D_x as defined by the authors is the absorbed dose that would demonstrate a x% probability in a tumour-response) was 160 Gy. The authors additionally remarked that the D_{mean}, and D_{20} to D_{80} values were able to predict an mRECIST response with significant correlation. For the normal liver, the authors found no significant correlations between the normal liver D_{mean} to the toxicities associated with bilirubin, albumin or ascites.

4. Conclusion

Radioembolization is a multi-faceted and multi-disciplinary treatment. With many clinical steps, the treatment process itself is highly personalized and theoretically compelling. However, the full effectiveness of the clinical plan has not yet been realized. One of the main drawbacks with this treatment is the basic and simplified dosimetry that is clinically practiced. The literature is further riddled with varying methods for dosimetric advances. Due to a myriad of inhomogeneous methodologies and dosimetric methods, patient responses based on quantified doses becomes challenging to interpret and compare. Therefore, proper standardized dosimetry becomes a necessary first step towards a sense of congruence and comparability. Primarily palliative, more first-line treatments must be conducted to truly test its effectiveness. Artery specific, thus tumour specific, effectiveness of a personalized treatment cannot be evaluated if the therapeutic goal is diffuse tumour ablations rather than tumour-targeted and curative plans. Fortunately, the continuing advancements of imaging modalities and the increasing power of computer technology permits faster and more accurate absorbed dose calculations. Higher resolution images and image based dosimetry methods (e.g. MC method) that take into account the patient's anatomy, tissue heterogeneities, proper detector calibrations, and accurate reconstruction techniques will eventually provide a complete and accurate dosimetry toolkit.

Disclosure

The authors have nothing to disclose.

Acknowledgments

This work was supported by the Collaborative Health Research Project (CHRP grant number 523394-18). The authors would like to thank Dr. Tatiana Cabrera at McGill University Health Center for her aid, which have allowed the firsthand participation in radioembolization planning steps and treatments.

Appendix A

Table 1
Recommended Radioembolization Studies.

Study*	Nature of Topic	Highlighted Content
[15]	Technical: Not Necessarily Review, but a Comprehensive Study	Covers Entire Procedure in Technical Detail • Has insight at every section
[13]	Recommendations by REBOC	Covers Entire Procedure • Read recommendations in Table 1
[8]	Recommendations and Overview of RE	Covers Entire Procedure in Technical Detail • Dosimetry Equations • ^{90}Y Calibration • Radiation Safety for patients, staff, and rooms
[5]	EANM Guidelines for ^{90}Yttrium Treatment	Covers Entire Treatment Procedure • Patient Indications • Administration • Dosimetry Equations • Comparisons between SIR- and Thera-Spheres
[6]	Review of Radiobiological and Dosimetric Methods	Covers Most Treatment Aspects of Radioembolization • Overall Microscopic Distribution • Radiobiological Modeling (EBRT vs. RE) • Radioembolization Side Effects (RILD vs. REILD, Thera vs. SIR-spheres, lungs) • Dose-response reports organized between Thera or SIR microsphere treatments
[12]	Recommendations on Safety and Activity Thresholds	Covers Entire Procedure • Treatment Planning Guide • Patient Activity Thresholds

(*continued on next page*)

Table 1 (*continued*)

Study*	Nature of Topic	Highlighted Content
[76]	Review of 3D Dosimetric Methods and Limitations for RE	Review Paper focusing on Dosimetry related Technicalities • Limitations of Dosimetry Equations • Image Based Dosimetry Methods (Monte Carlo, Dose Kernel Convolution, and Local Deposition) • Emerging Directions (PET scans, PET isotopes, other treatment isotopes)
[24]	Review of Radioembolization in General	Covers Every Treatment Aspect of Radioembolization • Clinical Indications, relative, and absolute contraindications • Tumour Response based primarily on clinical studies

* These papers include reviews, personal detailed accounts of the therapy, and recommendations for future radioembolization treatments.

References

[1] Roeske JC, Aydogan B, Bardies M, Humm JL. Small-scale dosimetry: challenges and future directions. Semin Nucl Med 2008;38:367–83.
[2] Kennedy AS, Nutting C, Coldwell D, Gaiser J, Drachenberg C. Pathologic response and microdosimetry of (90)Y microspheres in man: review of four explanted whole livers. Int J Radiat Oncol Biol Phys 2004;60:1552–63.
[3] Package insert-therapshere yttrium-90 glass microspheres. Biocompatibles UK Ltd, A BTG International Group Company.
[4] Package insert: sir-spheres microspheres. Sirtex Medical Limited; 2016. pp 9.
[5] Giammarile F, Bodei L, Chiesa C, Flux G, Forrer F, Kraeber-Bodere F, et al. EANM procedure guideline for the treatment of liver cancer and liver metastases with intra-arterial radioactive compounds. Eur J Nucl Med Mol Imaging 2011;38:1393–406.
[6] Cremonesi M, Chiesa C, Strigari L, Ferrari M, Botta F, Guerriero F, et al. Radioembolization of hepatic lesions from a radiobiology and dosimetric perspective. Front Oncol 2014;4:210.
[7] Coldwell D, Sangro B, Wasan H, Salem R, Kennedy A. General selection criteria of patients for radioembolization of liver tumors: an international working group report. Am J Clin Oncol 2011;34:337–41.
[8] Dezarn WA, Cessna JT, DeWerd LA, Feng W, Gates VL, Halama J, et al. American Association of Physicists in M: Recommendations of the American Association of Physicists in Medicine on dosimetry, imaging, and quality assurance procedures for 90Y microsphere brachytherapy in the treatment of hepatic malignancies. Med Phys 2011;38:4824–45.
[9] Ahmadzadehfar H, Meyer C, Pieper CC, Bundschuh R, Muckle M, Gartner F, et al. Evaluation of the delivered activity of yttrium-90 resin microspheres using sterile water and 5 % glucose during administration. EJNMMI Res 2015;5:54.
[10] Koran ME, Stewart S, Baker JC, Lipnik AJ, Banovac F, Omary RA, et al. Five percent dextrose maximizes dose delivery of Yttrium-90 resin microspheres and reduces rates of premature stasis compared to sterile water. Biomed Rep 2016;5:745–8.
[11] Kis B, Mills M, Hoffe SE. Hepatic radioembolization from transradial access: initial experience and comparison to transfemoral access. Diagn Interv Radiol 2016;22:444–9.
[12] Lau WY, Kennedy AS, Kim YH, Lai HK, Lee RC, Leung TW, et al. Patient selection and activity planning guide for selective internal radiotherapy with yttrium-90 resin microspheres. Int J Radiat Oncol Biol Phys 2012;82:401–7.
[13] Kennedy A, Nag S, Salem R, Murthy R, McEwan AJ, Nutting C, et al. Recommendations for radioembolization of hepatic malignancies using yttrium-90 microsphere brachytherapy: a consensus panel report from the radioembolization brachytherapy oncology consortium. Int J Radiat Oncol Biol Phys 2007;68:13–23.
[14] Riaz A, Awais R, Salem R. Side effects of yttrium-90 radioembolization. Front Oncol 2014;4:198.
[15] Salem R, Thurston KG. Radioembolization with 90Yttrium microspheres: a state-of-the-art brachytherapy treatment for primary and secondary liver malignancies. Part 1: technical and methodologic considerations. J Vasc Interv Radiol 2006;17:1251–78.
[16] Kennedy A. Radioembolization of hepatic tumors. J Gastrointest Oncol 2014;5:178–89.
[17] Vollmar B, Menger MD. The hepatic microcirculation: mechanistic contributions and therapeutic targets in liver injury and repair. Physiol Rev 2009;89:1269–339.
[18] Bierman HR, Byron Jr. RL, Kelley KH, Grady A. Studies on the blood supply of tumors in man. III. Vascular patterns of the liver by hepatic arteriography in vivo. J Natl Cancer Inst 1951;12:107–31.
[19] Van de Wiele C, Maes A, Brugman E, D'Asseler Y, De Spiegeleer B, Mees G, et al. SIRT of liver metastases: physiological and pathophysiological considerations. Eur J Nucl Med Mol Imaging 2012;39:1646–55.
[20] van den Hoven AF, Smits ML, de Keizer B, van Leeuwen MS, van den Bosch MA, Lam MG. Identifying aberrant hepatic arteries prior to intra-arterial radioembolization. Cardiovasc Intervent Radiol 2014;37:1482–93.
[21] Michels NA. Newer anatomy of the liver and its variant blood supply and collateral circulation. Am J Surg 1966;112:337–47.
[22] Vesselle G, Petit I, Boucebci S, Rocher T, Velasco S, Tasu JP. Radioembolization with yttrium-90 microspheres work up: Practical approach and literature review. Diagn Interv Imaging 2015;96:547–62.
[23] Uliel L, Royal HD, Darcy MD, Zuckerman DA, Sharma A, Saad NE. From the angio suite to the gamma-camera: vascular mapping and 99mTc-MAA hepatic perfusion imaging before liver radioembolization–a comprehensive pictorial review. J Nucl Med 2012;53:1736–47.
[24] Braat AJ, Smits ML, Braat MN, van den Hoven AF, Prince JF, de Jong HW, et al. (9)(0)Y hepatic radioembolization: an update on current practice and recent developments. J Nucl Med 2015;56:1079–87.
[25] Kao YH, Magsombol BM, Toh Y, Tay KH, Chow P, Goh AS, et al. Personalized predictive lung dosimetry by technetium-99m macroaggregated albumin SPECT/CT for yttrium-90 radioembolization. EJNMMI Res 2014;4:33.
[26] Hamami ME, Poeppel TD, Muller S, Heusner T, Bockisch A, Hilgard P, et al. SPECT/CT with 99mTc-MAA in radioembolization with 90Y microspheres in patients with hepatocellular cancer. J Nucl Med 2009;50:688–92.
[27] Allred JD, Niedbala J, Mikell JK, Owen D, Frey KA, Dewaraja YK. The value of (99m)Tc-MAA SPECT/CT for lung shunt estimation in (90)Y radioembolization: a phantom and patient study. EJNMMI Res 2018;8:50.
[28] Barentsz MW, Vente MA, Lam MG, Smits ML, Nijsen JF, Seinstra BA, et al. Technical solutions to ensure safe yttrium-90 radioembolization in patients with initial extrahepatic deposition of (99m)technetium-albumin macroaggregates. Cardiovasc Intervent Radiol 2011;34:1074–9.
[29] Lopez B, Mahvash A, Lam M, Kappadath SC. Calculation of lung mean dose and quantification of error for (90) Y-microsphere radioembolization using (99m) Tc-MAA SPECT/CT and diagnostic chest CT. Med Phys 2019;46:3929–40.
[30] Strasberg SM, Belghiti J, Clavien P-A, Gadzijev E, Garden JO, Lau W-Y, et al. The Brisbane 2000 terminology of liver anatomy and resections. HPB 2000;2(3):333–9.
[31] Germain T, Favelier S, Cercueil JP, Denys A, Krause D, Guiu B. Liver segmentation: practical tips. Diagn Interv Imaging 2014;95:1003–16.
[32] Vouche M, Lewandowski RJ, Atassi R, Memon K, Gates VL, Ryu RK, et al. Radiation lobectomy: time-dependent analysis of future liver remnant volume in unresectable liver cancer as a bridge to resection. J Hepatol 2013;59:1029–36.
[33] Seidensticker R, Seidensticker M, Damm R, Mohnike K, Schutte K, Malfertheiner P, et al. Hepatic toxicity after radioembolization of the liver using (90)Y-microspheres: sequential lobar versus whole liver approach. Cardiovasc Intervent Radiol 2012;35:1109–18.
[34] Lewandowski RJ, Donahue L, Chokechanachaisakul A, Kulik L, Mouli S, Caicedo J, et al. (90) Y radiation lobectomy: Outcomes following surgical resection in patients with hepatic tumors and small future liver remnant volumes. J Surg Oncol 2016;114:99–105.
[35] Riaz A, Gates VL, Atassi B, Lewandowski RJ, Mulcahy MF, Ryu RK, et al. Radiation segmentectomy: a novel approach to increase safety and efficacy of radioembolization. Int J Radiat Oncol Biol Phys 2011;79:163–71.
[36] Wondergem M, Smits ML, Elschot M, de Jong HW, Verkooijen HM, van den Bosch MA, et al. 99mTc-macroaggregated albumin poorly predicts the intrahepatic distribution of 90Y resin microspheres in hepatic radioembolization. J Nucl Med 2013;54:1294–301.
[37] Gulec SA, Mesoloras G, Stabin M. Dosimetric techniques in 90Y-microsphere therapy of liver cancer: The MIRD equations for dose calculations. J Nucl Med 2006;47:1209–11.
[38] Ho S, Lau WY, Leung TW, Chan M, Johnson PJ, Li AK. Clinical evaluation of the partition model for estimating radiation doses from yttrium-90 microspheres in the treatment of hepatic cancer. Eur J Nucl Med 1997;24:293–8.
[39] Leung TW, Lau WY, Ho SK, Ward SC, Chow JH, Chan MS, et al. Radiation pneumonitis after selective internal radiation treatment with intraarterial 90yttrium-microspheres for inoperable hepatic tumors. Int J Radiat Oncol Biol Phys 1995;33:919–24.
[40] Leung WT, Lau WY, Ho SK, Chan M, Leung NW, Lin J, et al. Measuring lung shunting in hepatocellular carcinoma with intrahepatic-arterial technetium-99m macroaggregated albumin. J Nucl Med 1994;35:70–3.
[41] Smits ML, Elschot M, Sze DY, Kao YH, Nijsen JF, Iagaru AH, et al. Radioembolization dosimetry: the road ahead. Cardiovasc Intervent Radiol 2015;38:261–9.
[42] Vauthey JN, Abdalla EK, Doherty DA, Gertsch P, Fenstermacher MJ, Loyer EM, et al. Body surface area and body weight predict total liver volume in Western adults. Liver Transpl 2002;8:233–40.
[43] Lam MG, Louie JD, Abdelmaksoud MH, Fisher GA, Cho-Phan CD, Sze DY. Limitations of body surface area-based activity calculation for radioembolization of hepatic metastases in colorectal cancer. J Vasc Interv Radiol 2014;25:1085–93.
[44] Grosser OS, Ulrich G, Furth C, Pech M, Ricke J, Amthauer H, et al. Intrahepatic activity distribution in radioembolization with yttrium-90-labeled resin microspheres using the body surface area method–a less than perfect model. J Vasc Interv

Radiol 2015;26:1615–21.
[45] Kao YH, Tan EH, Ng CE, Goh SW. Clinical implications of the body surface area method versus partition model dosimetry for yttrium-90 radioembolization using resin microspheres: a technical review. Ann Nucl Med 2011;25:455–61.
[46] Ho S, Lau WY, Leung TW, Chan M, Ngar YK, Johnson PJ, et al. Partition model for estimating radiation doses from yttrium-90 microspheres in treating hepatic tumours. Eur J Nucl Med 1996;23:947–52.
[47] Kao YH, Hock Tan AE, Burgmans MC, Irani FG, Khoo LS, Gong Lo RH, et al. Image-guided personalized predictive dosimetry by artery-specific SPECT/CT partition modeling for safe and effective 90Y radioembolization. J Nucl Med 2012;53:559–66.
[48] Mikell JK, Mahvash A, Siman W, Baladandayuthapani V, Mourtada F, Kappadath SC. Selective internal radiation therapy with yttrium-90 glass microspheres: biases and uncertainties in absorbed dose calculations between clinical dosimetry models. Int J Radiat Oncol Biol Phys 2016;96:888–96.
[49] Hashikin NAA, Yeong CH, Guatelli S, Abdullah BJJ, Ng KH, Malaroda A, et al. Systematic investigation on the validity of partition model dosimetry for (90)Y radioembolization using Monte Carlo simulation. Phys Med Biol 2017;62:7342–56.
[50] Oda M, Yokomori H, Han JY. Regulatory mechanisms of hepatic microcirculation. Clin Hemorheol Microcirc 2003;29:167–82.
[51] Fox RA, Klemp PF, Egan G, Mina LL, Burton MA, Gray BN. Dose distribution following selective internal radiation therapy. Int J Radiat Oncol Biol Phys 1991;21:463–7.
[52] Campbell AM, Bailey IH, Burton MA. Analysis of the distribution of intra-arterial microspheres in human liver following hepatic yttrium-90 microsphere therapy. Phys Med Biol 2000;45:1023–33.
[53] Campbell AM, Bailey IH, Burton MA. Tumour dosimetry in human liver following hepatic yttrium-90 microsphere therapy. Phys Med Biol 2001;46:487–98.
[54] Hogberg J, Rizell M, Hultborn R, Svensson J, Henrikson O, Molne J, et al. Heterogeneity of microsphere distribution in resected liver and tumour tissue following selective intrahepatic radiotherapy. EJNMMI Res 2014;4:48.
[55] Hogberg J, Rizell M, Hultborn R, Svensson J, Henrikson O, Molne J, et al. Increased absorbed liver dose in Selective Internal Radiation Therapy (SIRT) correlates with increased sphere-cluster frequency and absorbed dose inhomogeneity. EJNMMI Phys 2015;2:10.
[56] Lam MG, Louie JD, Iagaru AH, Goris ML, Sze DY. Safety of repeated yttrium-90 radioembolization. Cardiovasc Intervent Radiol 2013;36:1320–8.
[57] Lewandowski RJ, Minocha J, Memon K, Riaz A, Gates VL, Ryu RK, et al. Sustained safety and efficacy of extended-shelf-life (90)Y glass microspheres: long-term follow-up in a 134-patient cohort. Eur J Nucl Med Mol Imaging 2014;41:486–93.
[58] Walrand S, Hesse M, Chiesa C, Lhommel R, Jamar F. The low hepatic toxicity per Gray of 90Y glass microspheres is linked to their transport in the arterial tree favoring a nonuniform trapping as observed in posttherapy PET imaging. J Nucl Med 2014;55:135–40.
[59] Walrand S, Hesse M, Jamar F, Lhommel R. A hepatic dose-toxicity model opening the way toward individualized radioembolization planning. J Nucl Med 2014;55:1317–22.
[60] Gulec SA, Sztejnberg ML, Siegel JA, Jevremovic T, Stabin M. Hepatic structural dosimetry in (90)Y microsphere treatment: a Monte Carlo modeling approach based on lobular microanatomy. J Nucl Med 2010;51:301–10.
[61] Pasciak AS, Bourgeois AC, Bradley YC. A microdosimetric analysis of absorbed dose to tumor as a function of number of microspheres per unit volume in 90Y radioembolization. J Nucl Med 2016;57:1020–6.
[62] Van Audenhaege K, Van Holen R, Vandenberghe S, Vanhove C, Metzler SD, Moore SC. Review of SPECT collimator selection, optimization, and fabrication for clinical and preclinical imaging. Med Phys 2015;42:4796–813.
[63] Bailey DL, Willowson KP. Quantitative SPECT/CT: SPECT joins PET as a quantitative imaging modality. Eur J Nucl Med Mol Imaging 2014;41(Suppl. 1):S17–25.
[64] Siman W, Mikell JK, Kappadath SC. Practical reconstruction protocol for quantitative (90)Y bremsstrahlung SPECT/CT. Med Phys 2016;43:5093.
[65] Rong X, Du Y, Frey EC. A method for energy window optimization for quantitative tasks that includes the effects of model-mismatch on bias: application to Y-90 bremsstrahlung SPECT imaging. Phys Med Biol 2012;57:3711–25.
[66] Li T, Ao ECI, Lambert B, Brans B, Vandenberghe S, Mok GSP. Quantitative imaging for targeted radionuclide therapy dosimetry – technical review. Theranostics 2017;7:4551–65.
[67] Elschot M, Lam MG, van den Bosch MA, Viergever MA, de Jong HW. Quantitative Monte Carlo-based 90Y SPECT reconstruction. J Nucl Med 2013;54:1557–63.
[68] Rong X, Du Y, Ljungberg M, Rault E, Vandenberghe S, Frey EC. Development and evaluation of an improved quantitative (90)Y bremsstrahlung SPECT method. Med Phys 2012;39:2346–58.
[69] Dewaraja YK, Chun SY, Srinivasa RN, Kaza RK, Cuneo KC, Majdalany BS, et al. Improved quantitative (90) Y bremsstrahlung SPECT/CT reconstruction with Monte Carlo scatter modeling. Med Phys 2017;44:6364–76.
[70] Lhommel R, Goffette P, Van den Eynde M, Jamar F, Pauwels S, Bilbao JI, et al. Yttrium-90 TOF PET scan demonstrates high-resolution biodistribution after liver SIRT. Eur J Nucl Med Mol Imaging 2009;36:1696.
[71] Gates VL, Esmail AA, Marshall K, Spies S, Salem R. Internal pair production of 90Y permits hepatic localization of microspheres using routine PET: proof of concept. J Nucl Med 2011;52:72–6.
[72] Willowson KP, Tapner M, Team QI, Bailey DL. A multicentre comparison of quantitative (90)Y PET/CT for dosimetric purposes after radioembolization with resin microspheres: the QUEST Phantom Study. Eur J Nucl Med Mol Imaging 2015;42:1202–22.
[73] Yue J, Mauxion T, Reyes DK, Lodge MA, Hobbs RF, Rong X, et al. Comparison of quantitative Y-90 SPECT and non-time-of-flight PET imaging in post-therapy radioembolization of liver cancer. Med Phys 2016;43:5779.
[74] Elschot M, Vermolen BJ, Lam MG, de Keizer B, van den Bosch MA, de Jong HW. Quantitative comparison of PET and Bremsstrahlung SPECT for imaging the in vivo yttrium-90 microsphere distribution after liver radioembolization. PLoS One 2013;8:e55742.
[75] Kao YH, Steinberg JD, Tay YS, Lim GK, Yan J, Townsend DW, et al. Post-radioembolization yttrium-90 PET/CT - part 1: diagnostic reporting. EJNMMI Res 2013;3:56.
[76] Od J. A review of 3D image-based dosimetry, technical considerations and emerging perspectives in (90)Y microsphere therapy. J Diagn Imaging Ther 2015;2:1–34.
[77] Mikell JK, Mahvash A, Siman W, Mourtada F, Kappadath SC. Comparing voxel-based absorbed dosimetry methods in tumors, liver, lung, and at the liver-lung interface for (90)Y microsphere selective internal radiation therapy. EJNMMI Phys 2015;2:16.
[78] Gallio E, Richetta E, Finessi M, Stasi M, Pellerito RE, Bisi G, et al. Calculation of tumour and normal tissue biological effective dose in (90)Y liver radioembolization with different dosimetric methods. Phys Med 2016;32:1738–44.
[79] Lanconelli N, Pacilio M, Lo Meo S, Botta F, Di Dia A, Aroche AT, et al. A free database of radionuclide voxel S values for the dosimetry of nonuniform activity distributions. Phys Med Biol 2012;57:517–33.
[80] Campbell JM, Wong CO, Muzik O, Marples B, Joiner M, Burmeister J. Early dose response to yttrium-90 microsphere treatment of metastatic liver cancer by a patient-specific method using single photon emission computed tomography and positron emission tomography. Int J Radiat Oncol Biol Phys 2009;74:313–20.
[81] Kao YH. A clinical dosimetric perspective uncovers new evidence and offers new insight in favor of 99mTc-macroaggregated albumin for predictive dosimetry in 90Y resin microsphere radioembolization. J Nucl Med 2013;54:2191–2.
[82] Lam MG, Wondergem M, Elschot M, Smits ML. Reply: A clinical dosimetric perspective uncovers new evidence and offers new insight in favor of 99mTc-macroaggregated albumin for predictive dosimetry in 90Y resin microsphere radioembolization. J Nucl Med 2013;54:2192–3.
[83] Ulrich G, Dudeck O, Furth C, Ruf J, Grosser OS, Adolf D, et al. Predictive value of intratumoral 99mTc-macroaggregated albumin uptake in patients with colorectal liver metastases scheduled for radioembolization with 90Y-microspheres. J Nucl Med 2013;54:516–22.
[84] Fournier L, Ammari S, Thiam R, Cuenod CA. Imaging criteria for assessing tumour response: RECIST, mRECIST, Cheson. Diagn Interv Imaging 2014;95:689–703.
[85] Kao YH. Results confounded by a disregard for basic dose-response radiobiology. J Nucl Med 2013;54:1682–3.
[86] Lam MG, Smits ML. Value of 99mTc-macroaggregated albumin SPECT for radioembolization treatment planning. J Nucl Med 2013;54:1681–2.
[87] Garin E, Lenoir L, Rolland Y, Edeline J, Mesbah H, Laffont S, et al. Dosimetry based on 99mTc-macroaggregated albumin SPECT/CT accurately predicts tumor response and survival in hepatocellular carcinoma patients treated with 90Y-loaded glass microspheres: preliminary results. J Nucl Med 2012;53:255–63.
[88] Gnesin S, Canetti L, Adib S, Cherbuin N, Silva Monteiro M, Bize P, et al. Partition model-based 99mTc-MAA SPECT/CT predictive dosimetry compared with 90Y TOF PET/CT posttreatment dosimetry in radioembolization of hepatocellular carcinoma: a quantitative agreement comparison. J Nucl Med 2016;57:1672–8.
[89] Song YS, Paeng JC, Kim HC, Chung JW, Cheon GJ, Chung JK, et al. PET/CT-based dosimetry in 90Y-microsphere selective internal radiation therapy: single cohort comparison with pretreatment planning on (99m)Tc-MAA imaging and correlation with treatment efficacy. Medicine (Baltimore) 2015;94:e945.
[90] D'Arienzo M, Chiaramida P, Chiacchiararelli L, Coniglio A, Cianni R, Salvatori R, et al. 90Y PET-based dosimetry after selective internal radiotherapy treatments. Nucl Med Commun 2012;33:633–40.
[91] D'Arienzo M, Filippi L, Chiaramida P, Chiacchiararelli L, Cianni R, Salvatori R, et al. Absorbed dose to lesion and clinical outcome after liver radioembolization with 90Y microspheres: a case report of PET-based dosimetry. Ann Nucl Med 2013;27:676–80.
[92] Kao YH, Steinberg JD, Tay YS, Lim GK, Yan J, Townsend DW, et al. Post-radioembolization yttrium-90 PET/CT - part 2: dose-response and tumor predictive dosimetry for resin microspheres. EJNMMI Res 2013;3:57.
[93] Srinivas SM, Natarajan N, Kuroiwa J, Gallagher S, Nasr E, Shah SN, et al. Determination of radiation absorbed dose to primary liver tumors and normal liver tissue using post-radioembolization (90)Y PET. Front Oncol 2014;4:255.
[94] Strigari L, Sciuto R, Rea S, Carpanese L, Pizzi G, Soriani A, et al. Efficacy and toxicity related to treatment of hepatocellular carcinoma with 90Y-SIR spheres: radiobiologic considerations. J Nucl Med 2010;51:1377–85.
[95] Chan KT, Alessio AM, Johnson GE, Vaidya S, Kwan SW, Monsky W, et al. Prospective trial using internal pair-production positron emission tomography to establish the yttrium-90 radioembolization dose required for response of hepatocellular carcinoma. Int J Radiat Oncol Biol Phys 2018;101:358–65.
[96] Kappadath SC, Mikell J, Balagopal A, Baladandayuthapani V, Kaseb A, Mahvash A. Hepatocellular carcinoma tumor dose response after (90)Y-radioembolization with glass microspheres using (90)Y-SPECT/CT-based voxel dosimetry. Int J Radiat Oncol Biol Phys 2018;102:451–61.